Chemistry & Biology
Article

The Siderophore Binding Protein FeuA Shows Limited Promiscuity toward Exogenous Triscatecholates

Florian Peuckert,[1] Ana Laura Ramos-Vega,[1] Marcus Miethke,[1] Clemens J. Schwörer,[1] Alexander G. Albrecht,[1] Markus Oberthür,[1] and Mohamed A. Marahiel[1,*]
[1]Department of Chemistry, Biochemistry, Philipps-University Marburg, Hans-Meerwein-Straße, D-35032 Marburg, Germany
*Correspondence: marahiel@staff.uni-marburg.de
DOI 10.1016/j.chembiol.2011.05.006

SUMMARY

Iron acquisition by siderophores is crucial for survival and virulence of many microorganisms. Here, we investigated the binding of the exogenous siderophore ferric enterobactin and the synthetic siderophore mimic ferric mecam by the triscatecholate binding protein FeuA from *Bacillus subtilis* at the atomic level. The structural complexes provide molecular insights into the capture mechanism of FeuA for exogenous and synthetic siderophores. The protein-ligand complexes show an exclusive acceptance of Λ-stereoconfigured substrates. Ligand-induced cross-bridging of the complexes was not observed, revealing a different thermodynamic behavior especially of the ferric mecam substrate, which was previously shown to dimerize with the enterobactin binding protein CeuE. The nearly identical overall domain movement of FeuA upon binding of ferric enterobactin or ferric mecam compared with endogenously derived ferric bacillibactin implies the importance of the conserved domain rearrangement for recognition by the transmembrane permease FeuBC, for which the conserved FeuA residues E90 and E221 were proved to be essential.

INTRODUCTION

Iron acquisition is a major challenge for microbial species, regarding its very low bioavailability for both pathogenic and nonpathogenic strains (free iron[III] concentration of $\sim 10^{-24}$ M in serum; Carrano and Raymond, 1979) and 10^{-9} to 10^{-18} M in the environment at neutral pH (Chipperfield and Ratledge, 2000; Raymond and Carrano, 1979). Among several evolved strategies, one of the most prominent ways to overcome iron deprivation is the secretion of siderophores and their subsequent reimport in complex with iron(III) (Miethke and Marahiel, 2007). These low-molecular-weight organic compounds possess extraordinary high affinities toward ferric iron (up to 10^{48} M^{-1} for bacillibactin (BB) (Dertz et al., 2006) and 10^{49} M^{-1} for enterobactin (Ent) (Loomis and Raymond, 1991)).

Siderophores secreted by pathogenic bacteria are critical for their survival in mammalian hosts whose iron homeostasis is strictly regulated; therefore siderophores often represent virulence factors. The innate immune defense protein siderocalin (also referred to as lipocalin 2 or neutrophile gelatinase associated lipocalin (NGAL)) is involved in the sequestration of iron bound by catecholate siderophores (Goetz et al., 2002), catecholamines (Miethke and Skerra, 2010) or even catechole (Bao et al., 2010), thereby reducing the pool of available iron for pathogens. This defense mechanism is directed against the most prominent siderophores: enterobactin from Gram-negative bacteria (Goetz et al., 2002), bacillibactin from Gram-positive bacteria (Abergel et al., 2006), and carboxymycobactins from mycobacteria (Holmes et al., 2005).

Bacteria also use low-affinity siderophore precursors, such as 2,3-dihydroxybenzoate (2,3-DHB) by *Bacillus subtilis* (Peters and Warren, 1968) and *Escherichia coli* (Hancock et al., 1977), and 3,4-dihydroxybenzoate (3,4-DHB) by *Bacillus anthracis* (Garner et al., 2004) to complex ferric ions. However, an additional common survival strategy of pathogenic and nonpathogenic bacteria is the capture of siderophores which are not produced by themselves, so-called exogenous, or xeno-siderophores.

The Gram-positive model organism *B. subtilis* utilizes bacillibactin as endogenous siderophore (May et al., 2001; Miethke et al., 2006) and can further import the exogenous siderophores enterobactin, petrobactin, or hydroxamate-type siderophores such as ferrichrome or schizokinen (Ollinger et al., 2006; Zawadzka et al., 2009).

Siderophore import in bacteria is accomplished by complex transport machineries. Gram-negative bacteria possess highly specialized β-barrel-shaped outer membrane receptors, which bind a specific siderophore, such as FepA for ferric enterobactin or FhuA for ferric hydroxamates (Braun and Braun, 2002; Chakraborty et al., 2007). Further transport from the periplasm to the cytoplasm is carried out by ATP-binding cassette-type (ABC) transporters, which comprise two transmembrane permease components, two nucleotide-binding domains, and a periplasmic binding protein. In Gram-positive bacteria, the periplasmic binding proteins are substituted by so-called substrate binding proteins (SBPs), which are tethered to the cytoplasmic membrane by lipid anchors. SBPs from both Gram-negative and Gram-positive bacteria are generally more promiscuous than the outer membrane receptors of Gram-negative bacteria and may transport a whole class of siderophores, rather than one specific compound (Krewulak and Vogel, 2008).

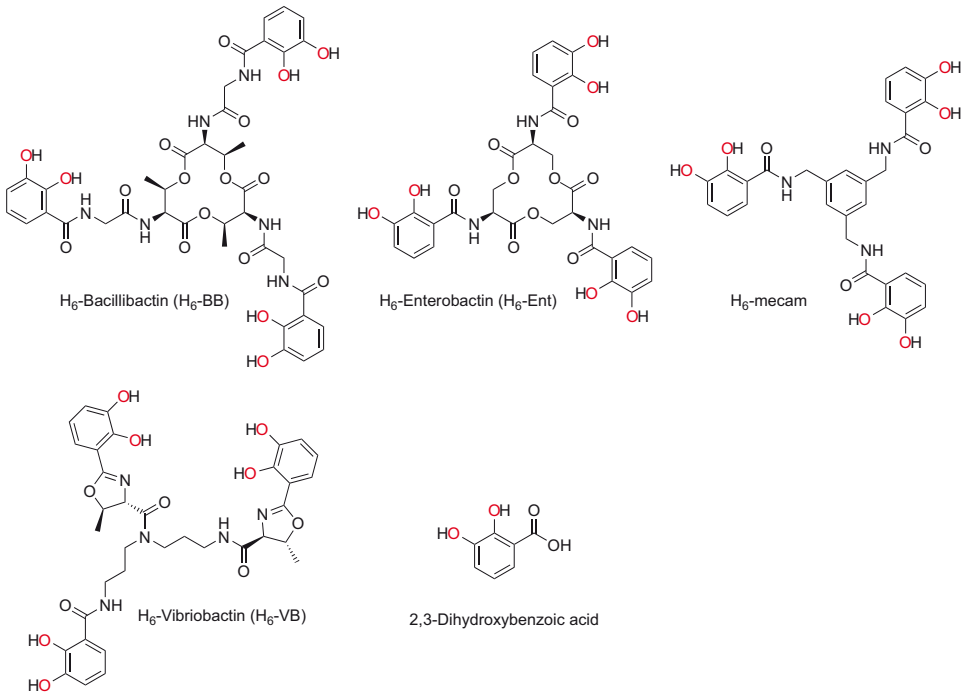

Figure 1. Structures of Prominent Triscatecholate Siderophores
Shown are the triscatecholate siderophores bacillibactin, enterobactin, and vibriobactin, the triscatecholate siderophore mimeticum mecam, and the precursor 2,3-dihydroxybenzoic acid. The iron coordinating groups are shown in red.

The FeuABC-YusV$_2$ transporter of *B. subtilis* was shown to import ferric complexes of both bacillibactin and enterobactin (Miethke et al., 2006; Ollinger et al., 2006). Recently, we solved the structure of the FeuA·[Fe^{III}(BB)]$^{3-}$ complex at 1.70 Å resolution (Peuckert et al., 2009), which revealed a basic triad composed of K84, K105, and R180 to be mainly responsible for binding of the ligand. The C-terminal domain of FeuA shifts about 20° relative to the N-terminal domain when the ligand is bound, which is the largest known domain movement for a member of the "helical-backbone" metal-receptor superfamily, the so-called class III. Ferric bacillibactin was found in its Λ-stereoconfiguration in the *holo*-FeuA structure. Further, the ferric complexes of enterobactin and the triscatecholate siderophore mimic mecam (H$_6$-mecam = 1,3,5-*N*,*N*′,*N*″-tris[2,3-dihydroxybenzoyl]triaminomethylbenzene) showed a Λ-stereoconfiguration when bound by FeuA in solution (Peuckert et al., 2009). In contrast, free-solvated ferric enterobactin was shown to adopt a Δ-configuration (Karpishin et al., 1993).

To elucidate the structure-functional relationship of xenosiderophore binding, we investigated the structural basis for the substrate promiscuity of FeuA, in regard to the exogenous siderophore enterobactin, and its nonhydrolyzable synthetic analog, mecam. Cocrystal structures of the FeuA·[Fe^{III}(Ent)]$^{3-}$ and FeuA·[Fe^{III}(mecam)]$^{3-}$ complexes provide structural insights into the binding modes of structurally related triscatecholate substrates. Binding of further distantly related siderophores including vibriobactin (VB) and 2,3-DHB (Figure 1) was additionally studied by spectroscopic measurements in solution.

RESULTS

Overall Structures

The complexes of FeuA with [Fe^{III}(Ent)]$^{3-}$ and [Fe^{III}(mecam)]$^{3-}$ both crystallized in space group $P2_1$, as did the FeuA·[Fe^{III}(BB)]$^{3-}$ complex (PDB code: 2WHY) reported previously (Peuckert et al., 2009). The crystals were obtained under similar conditions; the cell dimensions are similar to those of the known complex and contain also one monomer per asymmetric unit. Both structures were solved by molecular replacement using the structure of the FeuA·[Fe^{III}(BB)]$^{3-}$ complex as a model and X-ray data to a resolution of 1.90 Å for FeuA·[Fe^{III}(Ent)]$^{3-}$ and of 2.15 Å for FeuA·[Fe^{III}(mecam)]$^{3-}$. Detailed data collection and refinement statistics are given in Table 1; the overall structures of both complexes are shown in Figures 2A and 2B.

Residues 1–18 in the N-terminal domain of the mature protein and 300–305 in the C-terminal domain of FeuA·[Fe^{III}(Ent)]$^{3-}$ and 1–17 and 301–305 of FeuA·[Fe^{III}(mecam)]$^{3-}$ could not be modeled, as was already the case for the FeuA·[Fe^{III}(BB)]$^{3-}$ structure. This is most likely due to disorder in the N- and C-terminal regions, which was predicted using the DISOPRED2 server (Ward et al., 2004).

Both complexes are remarkably similar to the FeuA·[Fe^{III}(BB)]$^{3-}$ complex. The domain tilting upon ligand binding is 20.8° for the [Fe^{III}(Ent)]$^{3-}$ and 20.4° for the [Fe^{III}(mecam)]$^{3-}$ complex, which is comparable to the 20.2° shift observed for the FeuA·[Fe^{III}(BB)]$^{3-}$ complex compared with *apo*-FeuA (PDB code: 2WI8). When overlaying the N-terminal domains, *apo*- and *holo*-FeuA can be clearly discriminated by the distance

Table 1. Crystallographic Data Collection and Refinement Statistics

Data Processing	FeuA·[Fe^{III}(Ent)]$^{3-}$	FeuA·[Fe^{III}(mecam)]$^{3-}$
PDB code	2XUZ	2XV1
Beamline	ID14-2, ESRF	ID14-2, ESRF
Wavelength (Å)	0.933	0.933
Detector	ADSC Q4 CCD	ADSC Q4 CCD
Space group	$P2_1$	$P2_1$
a, *b*, *c* (Å)	36.44, 63.56, 56.52; β = 100.65°	39.96, 63.44, 56.21; β = 110.27°
Resolution (Å)	41.83–1.90	40.55–2.15
Total reflections[a]	61,441 (8791)	41,311 (6091)
Unique reflections[a]	19,907 (2852)	13,962 (2074)
Completeness[a]	99.1 (97.7)	96.9 (98.3)
$\langle I \rangle / \sigma\langle I \rangle$[a]	14.8 (2.5)	18.4 (2.2)
R_{merge}[a,b]	0.058 (0.493)	0.046 (0.595)
Mosaicity (°)	0.520	0.251
Wilson *B* factor (Å^2)	21.4	39.1
Refinement		
R_{work}, R_{free}[c,d]	18.47, 24.32	17.81, 23.66
Used reflections	18,136	12,740
Mean *B* factor (Å^2)	22.4	38.3
No. of atoms	2430	2314
Rmsd from ideal		
Bond lengths (Å)	0.0091	0.0084
Bond angles (°)	1.213	1.142

[a] Values in parentheses correspond to the highest resolution shell.
[b] $R_{merge} = \Sigma_{hkl} \Sigma_i (I_i(hkl) - < I(hkl) >) / \Sigma_{hkl} \Sigma_i I_i(hkl)$.
[c] $R_{work} = \Sigma (F_{obs}\text{-}F_{calc}) / \Sigma (F_{obs})$.
[d] R_{free} crystallographic R factor based on 5.0% (FeuA·[Fe^{III}(Ent)]$^{3-}$) and 7.2% (FeuA·[Fe^{III}(mecam)]$^{3-}$), respectively, of the data withheld from the refinement for cross-validation.

between the two conserved glutamate residues E90 and E221, which are assumed to form salt bridges with conserved arginine residues of the transmembrane permease components FeuB (R59) and FeuC (R53), thereby triggering the substrate translocation through the cytoplasmic membrane. This attribution is based on similar observations for the vitamin B_{12} (Btu) (Borths et al., 2002; Hvorup et al., 2007) and the ferric citrate (Fec) (Braun and Herrmann, 2007) uptake systems of *E. coli* and the ferric hydroxamate uptake system (Fhu) of *Staphylococcous aureus* (Sebulsky et al., 2003). The distance between E90 and E221 is 48.5 Å for *apo*-FeuA and 44.4 Å for *holo*-FeuA, with an angle of ~13° and a distance of 11.3 Å between *apo*- and *holo*-E221, calculated for the C_α atoms (Figure 2C).

The superposition of the complexes with FeuA·[Fe^{III}(BB)]$^{3-}$ reveals root mean square deviations of 0.38 Å for in total 278 C_α positions of FeuA·[Fe^{III}(Ent)]$^{3-}$ and 0.26 Å for in total 282 C_α positions of FeuA·[Fe^{III}(mecam)]$^{3-}$ (Figure 2D). Diverse structural elements were located mainly at the flexible N and C termini, most likely caused by differences in crystal packing, expressed in slightly different cell parameters.

As expected, both ligands are stabilizing the overall protein fold which is displayed by significantly increased melting temperatures, which were monitored by circular dichroism spectroscopy. The FeuA·[Fe^{III}(Ent)]$^{3-}$ and FeuA·[Fe^{III}(mecam)]$^{3-}$ complexes showed melting temperatures that are between 8°C and 10°C higher than that of *apo*-FeuA. These results are in the same range observed for FeuA·[Fe^{III}(BB)]$^{3-}$. In contrast, the ferric complexes of 2,3-DHB, Fe^{III}(2,3-DHB)$_3$, and of vibriobactin, [Fe^{III}(VB)]$^{3-}$, did not enhance the overall folding stability of FeuA (see Figure S1 available online).

Siderophore Binding

The FeuA·[Fe^{III}(BB)]$^{3-}$ complex revealed a basic triad, made up of K84 and K105 provided by the N-terminal domain and R180 from the C-terminal domain. Q181 and Q215 were the only other binding pocket forming residues, which showed additional direct interactions with the ligand by hydrogen bonding. However, the basic triad was shown to be mainly responsible for binding, as indicated by a drastic decrease of binding affinity, even if only one residue was substituted by alanine (Peuckert et al., 2009).

The two ligands [Fe^{III}(Ent)]$^{3-}$ and [Fe^{III}(mecam)]$^{3-}$ are bound in an analogous way. The SIGMAA-weighted (F_{obs}–F_{calc}) electron-density difference for these ligands is shown in Figures 3A and 3B.

The relative position of the ligands in the binding pocket is similar and the basic triad itself is well defined in both complexes and differs only little in its position and distances compared with the FeuA·[Fe^{III}(BB)]$^{3-}$ complex (Figures 3C and 3D; Table S1).

The most obvious changes appear at residues Q181 and Q215. In the FeuA·[Fe^{III}(Ent)]$^{3-}$ complex, the side chain of Q181 is rotated away from the binding pocket, resulting in an explicitly weakened hydrogen bond. Q215 exhibits extended distances to the *ortho*-oxygen atoms of the ligand, but forms an additional hydrogen bond from its main chain amide N-H to the carbonyl oxygen of one 2,3-DHB moiety. In the FeuA·[Fe^{III}(mecam)]$^{3-}$ complex, no electron density for the side chain of Q181 was observable, showing the loss of hydrogen bonds with the ligand. Q215 shows additional hydrogen bonding from its main chain amide N-H to the carbonyl oxygen of one 2,3-DHB moiety (Figure 3D; Tables S1 and S2).

All other residues in the binding pocket show insignificant changes and retain the overall shape and surface observed in the FeuA·[Fe^{III}(BB)]$^{3-}$ complex. A detailed list of all changes in the binding pocket can be found in the Tables S1 and S2.

Stereoconfiguration and Structural Features of the Ligands

Both complexes exhibit nearly C_3 point symmetry and adopt a Λ-configuration when bound by FeuA, which was already observed spectroscopically in solution (Peuckert et al., 2009). The ligands show trigonal twist angles of the three catecholate groups relative to their almost C_3 axes of 11.8°, 7.6°, and 10.8° for [Fe^{III}(Ent)]$^{3-}$ and 13.4°, 11.3°, and 12.3° for [Fe^{III}(mecam)]$^{3-}$, respectively. These twist angles generate an approximate octahedral iron coordination. The torsion of the metal-chelating DHB units of [Fe^{III}(Ent)]$^{3-}$ and [Fe^{III}(mecam)]$^{3-}$ is not as strong as observed for [Fe^{III}(BB)]$^{3-}$. It seems that the additional glycine spacer in bacillibactin (between the metal center and the trilactone moiety) generates further requirements concerning space, sterical hindrance and torsion angles, resulting in a slightly stronger tilting.

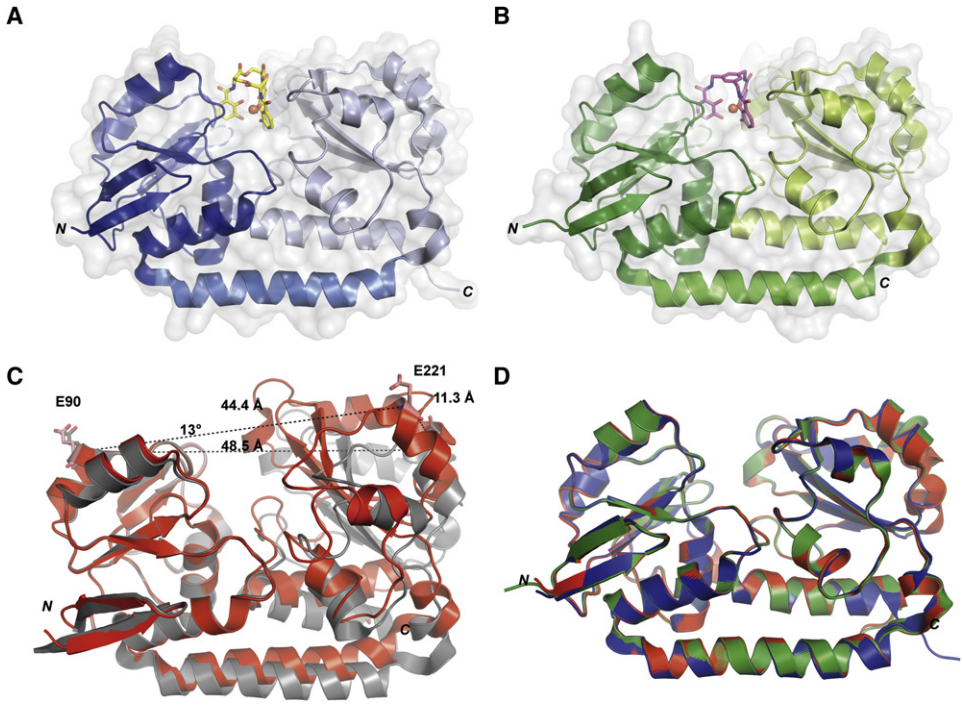

Figure 2. Overall Structures of FeuA-Siderophore Complexes

(A and B) The overall structures of (A) FeuA·$[Fe^{III}(Ent)]^{3-}$ and (B) FeuA·$[Fe^{III}(mecam)]^{3-}$. The N- and C-terminal domains and the connecting α helix of the protein backbone are shown in different shades of blue and green, respectively. The ligand atoms are colored as follows: *O* red, *N* blue, *Fe* orange sphere, *C* yellow and magenta, respectively.

(C) The N-terminal domains of *apo*- (gray) and *holo*-FeuA (red) were superpositioned. The distances between the conserved residues E90 and E221 are shown. See also Figure S1.

(D) Superposition of FeuA complexed with $[Fe^{III}(BB)]^{3-}$ (red), $[Fe^{III}(Ent)]^{3-}$ (blue) and $[Fe^{III}(mecam)]^{3-}$ (green). All Figures were created with PyMOL 1.3 (Schrödinger, 2010).

We also tested ferric complexes of the bacillibactin and enterobactin precursor 2,3-DHB and of the distantly related triscatecholate vibriobactin for absolute configurations at their metal centers. Negative bands around 450 nm and positive ones around 550 nm are indicative for iron-triscatecholate complexes with Λ-configuration (Bluhm et al., 2002b). Whereas FeuA was found to induce the formation of Λ-configured species in the racemic mixture of $Fe^{III}(2,3\text{-DHB})_3$, the configuration of the $[Fe^{III}(VB)]^{3-}$ complex remained unchanged (Figure 4). To determine the binding constants for the different ferric triscatecholate ligands, fluorescence titration experiments were performed with $[Fe^{III}(Ent)]^{3-}$, $[Fe^{III}(mecam)]^{3-}$, $Fe^{III}(2,3\text{-DHB})_3$, and $[Fe^{III}(VB)]^{3-}$. FeuA binds not only $[Fe^{III}(BB)]^{3-}$ with high affinity (K_D = 0.027 ± 0.001 μM) (Miethke and Skerra, 2010; Peuckert et al., 2009), but also $[Fe^{III}(Ent)]^{3-}$ (K_D = 0.04 ± 0.01 μM). Our affinity constant for $[Fe^{III}(Ent)]^{3-}$ is in good agreement with previously published data (Abergel et al., 2009; Miethke et al., 2006). The synthetic siderophore $[Fe^{III}(mecam)]^{3-}$ is bound with slightly lower affinity (K_D = 1.03 ± 0.03 μM), in contrast to the precursor $Fe^{III}(2,3\text{-DHB})_3$, which shows significantly weaker binding (K_D = 8.38 ± 0.26 μM) (Figure S4). For $[Fe^{III}(VB)]^{3-}$, only unspecific binding was observed. The low binding affinities for the two latter complexes are supported by the missing stabilization of the protein upon heat denaturation (Figure S2).

The crystal structure of the SBP CeuE from the foodborne pathogen *Campylobacter jejuni* revealed a dimeric $(CeuE)_2\cdot\{Fe^{III}(mecam)\}_2$ complex. Two CeuE monomers were bridged by a Λ,Λ-$[\{Fe^{III}(mecam)\}_2]^{6-}$ binuclear complex (Müller et al., 2006). Our structure, however, shows a single $[Fe^{III}(mecam)]^{3-}$ complex bound by one FeuA macromolecule and is therefore clearly different from the $(CeuE)_2\cdot\{Fe^{III}(mecam)\}_2$ complex. The monomeric nature of the complex in solution was also confirmed by size exclusion chromatography (data not shown). Ferric mecam bound by FeuA mimics the coordination mode and shape of a natural triscatecholate siderophore. The aromatic moiety which substitutes the trilactone ring of the natural siderophores enterobactin or bacillibactin is not recognized by the protein and, furthermore, does not form π–π interactions (for example, between two possibly head-to-head symmetry-related molecules within a crystal).

Comparison of Binding Residues

The only other structurally characterized SBPs for catecholate-type siderophores are the aforementioned CeuE from *C. jejuni* (Müller et al., 2006) and FpiA (YclQ) from *B. subtilis* (Bugdahn et al., 2010; Zawadzka et al., 2009), which binds the mixed catecholate–citrate siderophore petrobactin. The basic triad in CeuE is composed of R117, R204, and R248. The binding region of FpiA is lined with the basic residues K84, R104, R192, H214, and R236, which were predicted to participate in binding, based on comparison with the CeuE structure (Zawadzka et al., 2009).

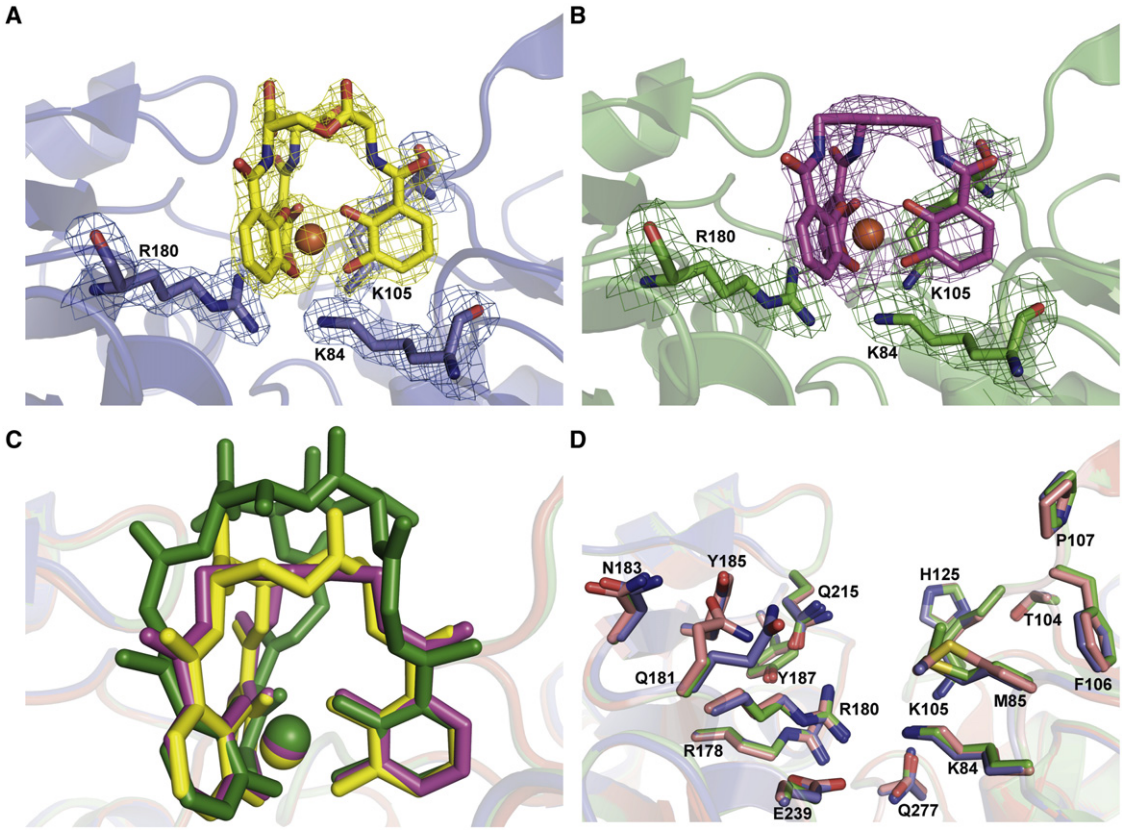

Figure 3. Siderophore Binding Pocket of FeuA

(A and B) SIGMAA-weighted (F_{obs}–F_{calc}) electron-density difference is shown for $[Fe^{III}(Ent)]^{3-}$ (yellow, contour level 2.7 σ, calculated at 1.90 Å resolution) and $[Fe^{III}(mecam)]^{3-}$ (magenta, contour level 2.7 σ, calculated at 2.15 Å resolution), respectively; $2F_{obs}$–F_{calc} electron density (blue and green, respectively, contour level 1 σ) is shown for residues K84, K105, and R180 (*C* light blue and light green, respectively). For ligand coloring, refer to Figure 2. See also Figures S2 and S3.

(C) Overlay of the three different ligands in the binding pocket: $[Fe^{III}(BB)]^{3-}$ (green), $[Fe^{III}(Ent)]^{3-}$ (yellow), and $[Fe^{III}(mecam)]^{3-}$ (magenta).

(D) Overlay of the residues of the first and second shell of the binding site for the triscatecholate ligands (*C* light red, light blue and light green for FeuA complexed with $[Fe^{III}(BB)]^{3-}$, $[Fe^{III}(Ent)]^{3-}$, and $[Fe^{III}(mecam)]^{3-}$, respectively). See also Tables S1 and S2.

An overlay of the structures of $(CeuE)_2 \cdot \{Fe^{III}(mecam)\}_2$ and $FeuA \cdot [Fe^{III}(mecam)]^{3-}$ shows clear differences in the positioning of both the ligand and the basic triad (Figure 5). The $[\{Fe^{III}(mecam)\}_2]^{6-}$ dimer in CeuE is bound more shallow in the binding pocket than $[Fe^{III}(mecam)]^{3-}$ in FeuA. While R204 and R248 in CeuE point upward from below the triscatecholate metal center, the basic triad in FeuA appears more from the same level or from above.

This tolerance in position of the crucial residues for siderophore binding supports the substrate promiscuity of SBPs. It seems that in addition to presence of the basic triad, the overall shape of the binding site is of similar importance for selection of a predefined substrate spectrum. Clarke et al. showed for the ferric hydroxamate siderophore binding protein FhuD, that even mutations in residues which only contribute to the overall fold of the binding site may impair siderophore recognition (Clarke et al., 2002b).

A multiple sequence alignment of known triscatecholate siderophore binding proteins is shown in Figure S6. Typical for class III SBPs is the conserved fold, while the homology at the sequence level is rather low (Table S3). The basic triad in the triscatecholate siderophore binding proteins FepB from *E. coli*, CeuE from *C. jejuni*, and VctP and ViuP from *Vibrio cholerae* is not well conserved.

Mutational and Growth Studies

The sequence alignment in Figure S6 shows the two glutamate residues E90 and E221 of FeuA, which are predicted to be responsible for interaction with the transmembrane permease FeuBC (interaction model, see Figure 6A). In contrast to the basic triad, these two residues are well conserved for all six examined proteins (the second glutamate residue in FpiA is substituted by aspartate). To verify the physiological role of the two residues, we performed mutational studies of the two residues in vivo. A *B. subtilis* Δ*feuABC* deletion mutant showed impaired growth compared with the wild-type ATCC 21332. This mutant was complemented with the native *feuABC* cluster or with a $feuA_{E90A,E221A}BC$ double mutated gene cluster. While western blot analysis confirmed a similar production of both FeuA variants, the $feuA_{E90A,E221A}BC$ complemented strain was not able to grow under iron-limited conditions, whereas the strain complemented with the native *feuABC* cluster showed stronger growth compared with the wild-type (Figure 6B). This proves the crucial role of E90 and E221 for the interaction with FeuBC

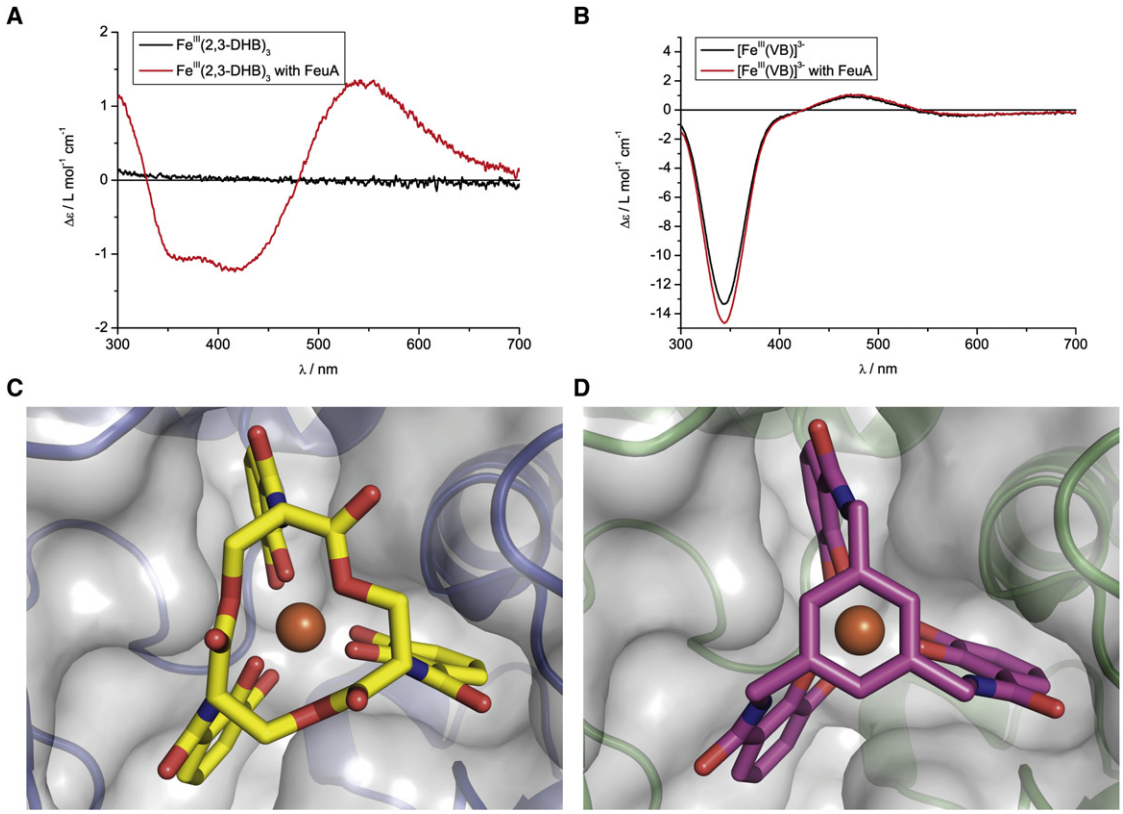

Figure 4. Stereoconfiguration of Ferric Triscatecholate Complexes

(A and B) Circular dichroism spectra of $Fe^{III}(2,3\text{-}DHB)_3$ and $[Fe^{III}(VB)]^{3-}$ in presence and absence of FeuA.

(C and D) Zoom on the $[Fe^{III}(Ent)]^{3-}$ and $[Fe^{III}(mecam)]^{3-}$ complexes in the FeuA binding pocket illustrating their Λ-configuration.

See also Figure S4.

and for the transport process itself, according to the model in Figure 6A. Fluorescence quenching analysis of the recombinant protein variant FeuA-E90A,E221A proved that the binding affinities for the ligands were in the same range as observed for the wild-type protein.

Furthermore, the physiological availability of the examined siderophores BB, Ent, and mecam to *B. subtilis* was tested by growth analysis (Figure 6C). While supplementation with native siderophores $[Fe^{III}(BB)]^{3-}$ and $[Fe^{III}(Ent)]^{3-}$ supported strongly the growth of a *B. subtilis* Δ*dhbC* mutant, which is unable to produce any catecholate compounds for iron acquisition (Miethke et al., 2006), $[Fe^{III}(mecam)]^{3-}$ provided a significantly lower growth promotion. The iron-free siderophores *apo*-BB and *apo*-Ent were also able to provide growth benefits to Δ*dhbC*, whereas the *apo*-mecam feeded cultures showed significantly impaired growth compared with the control experiments. The Δ*dhbC* Δ*feuABC* double mutant was drastically impaired in growth in presence of all triscatecholate supplements, demonstrating the essential and unique role of the FeuABC-$YusV_2$ system for triscatecholate-dependent iron acquisition in *B. subtilis* (Figure 6C).

DISCUSSION

The ABC-type transporter FeuABC-$YusV_2$ is responsible for triscatecholate siderophore import in *Bacillus subtilis*. We have recently shown that a basic triad composed of K84, K105, and R180 is responsible for $[Fe^{III}(BB)]^{3-}$ binding by FeuA, thereby allowing solely a Λ-configuration at the triscatecholate-metal center (Peuckert et al., 2009). In this work, we present cocrystal structures of FeuA with ferric complexes of the best studied siderophore enterobactin and the triscatecholate siderophore analog mecam. This siderophore mimic is of special interest, because it was reported to accumulate in the periplasm of *E. coli* and to have a significantly lower iron delivery ratio compared with Ent (Ecker et al., 1986; Matzanke et al., 1986), probably also due to its nonhydrolyzable backbone. The dimerization of the binding protein CeuE from *C. jejuni* by a $[\{Fe^{III}(mecam)\}_2]^{6-}$ dimer (Müller et al., 2006) also inspired a new inhibition strategy for such binding proteins (Miethke and Marahiel, 2007). Enterobactin on the other hand is a widely distributed siderophore, produced by several Gram-negative bacteria, such as *Escherichia coli*, *Salmonella enterica*, *Klebsiella* spp., and *Shigella* spp. Therefore, understanding the detailed capturing mode performed by a triscatecholate binding protein for this siderophore is a crucial issue for exploring its overall binding mechanism and furthermore, the interspecies competition for siderophores. Successful strategies require the development of high-affinity transport systems with broad substrate specificity. To establish cell surface receptors, which are able to directly compete with the highly specific outer membrane

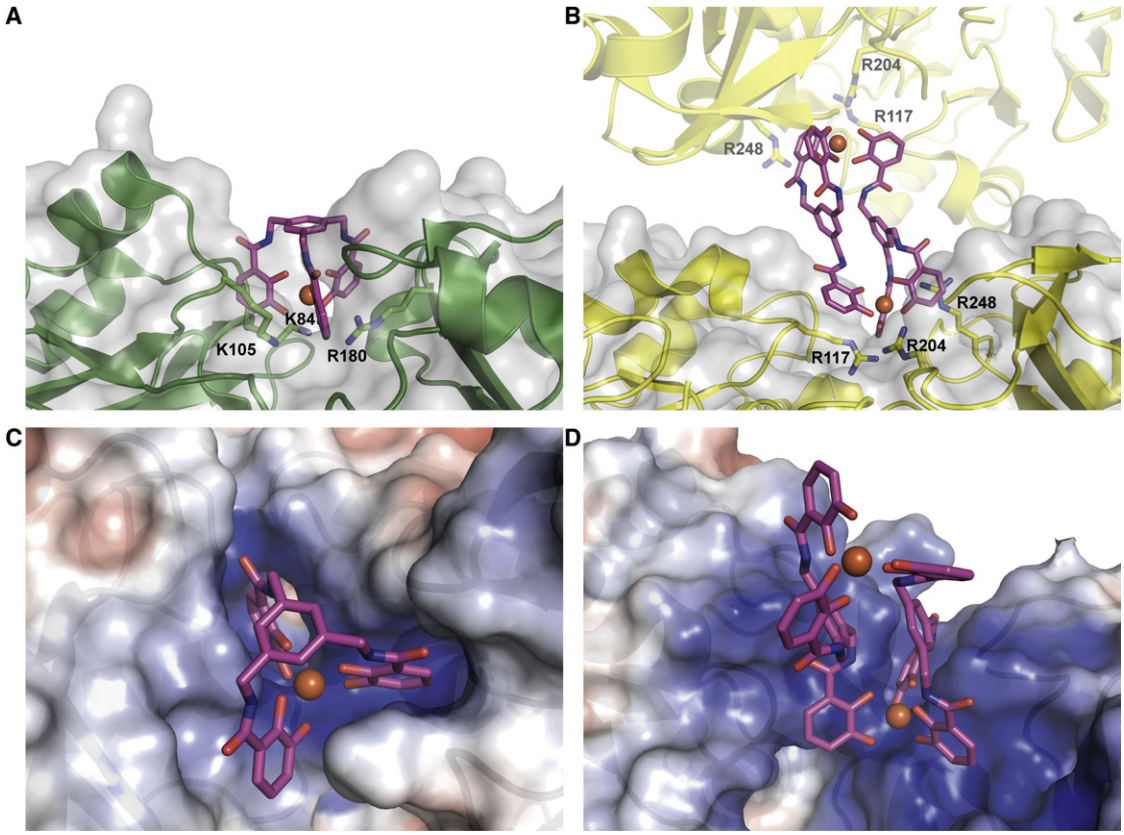

Figure 5. Comparison of FeuA and CeuE Binding Pockets

(A and B) Binding residues in FeuA (green) and CeuE (yellow) with the ligands $[Fe^{III}(mecam)]^{3-}$ and $[\{Fe^{III}(mecam)\}_2]^{6-}$ (for ligand coloring, refer to Figure 2), respectively.

(C and D) Electrostatic surface representation of the binding pockets (from −5 [red] to +5 [blue] k_BT/e_c), generated with APBS (Baker et al., 2001).

See also Figure S5.

transporters of Gram-negative bacteria, SBPs of Gram-positive bacteria typically possess affinities toward their substrate in a similar range.

The stabilization of FeuA by $[Fe^{III}(Ent)]^{3-}$ and $[Fe^{III}(mecam)]^{3-}$ against thermal denaturation is in a similar range compared with the endogenous substrate $[Fe^{III}(BB)]^{3-}$ and the overall structures of all three FeuA-ferrisiderophore complexes show no significant changes among each other, contrary to the great hinge motion between the *apo*- and *holo* structures. Large domain movements are well known for β strand-bridged SBPs of class I or II (e.g., 35° for the maltose binding protein; Sharff et al., 1992) and have therefore been termed the "venus flytrap" mechanism. The connecting α helix between the two domains in the "helical backbone" metal receptor superfamily is assumed to induce rigidity into the structure, resulting in significantly smaller domain tilting upon ligand binding. Accordingly, most examples of this superfamily show movements of only a few degrees. The domain motion is thought to be important for the specific recognition of SBPs by their cognate transmembrane permease.

The similar domain tilt in our three cocrystal structures emphasizes an important prerequisite for recognition of the conserved residues E90 and E221 by the transmembrane permease FeuBC. Our crystallographic analysis and furthermore the molecular dynamics simulations of FhuD (Krewulak et al., 2005) and BtuF (Kandt et al., 2006) as well as the recent structural characterization of the *E. coli* siderophore binding protein FitE (Shi et al., 2009) suggest that at least some class III SBPs are much more flexible than previously assumed. The recently determined *apo*- and *holo*-crystal structures of the staphyloferrin A and B binding proteins HtsA and SirA, respectively, from *Staphylococcus aureus* showed a very small domain movement, while the major conformational changes were accomplished by three loops of the C-terminal domains (Grigg et al., 2010a, 2010b). The structure of $BtuC_2D_2F$ reveals a much higher degree of domain tilting in BtuF, than in the *apo*-/*holo* structures (Borths et al., 2002; Hvorup et al., 2007; Karpowich et al., 2003). The different behaviors of these structurally related proteins suggest that the recognition of binding proteins by their cognate transmembrane permease is either different or much more complicated than previously assumed.

The similar structural motion seen in all of our cocrystal structures, implying a similar recognition and transport mechanism is provoked by the nearly identical binding mode of the related siderophores. The basic triad, crucial for binding of the negatively charged siderophore, differs slightly in its position. The basic triad seems to be the common binding motif of triscatecholate siderophore binding proteins and was also observed in

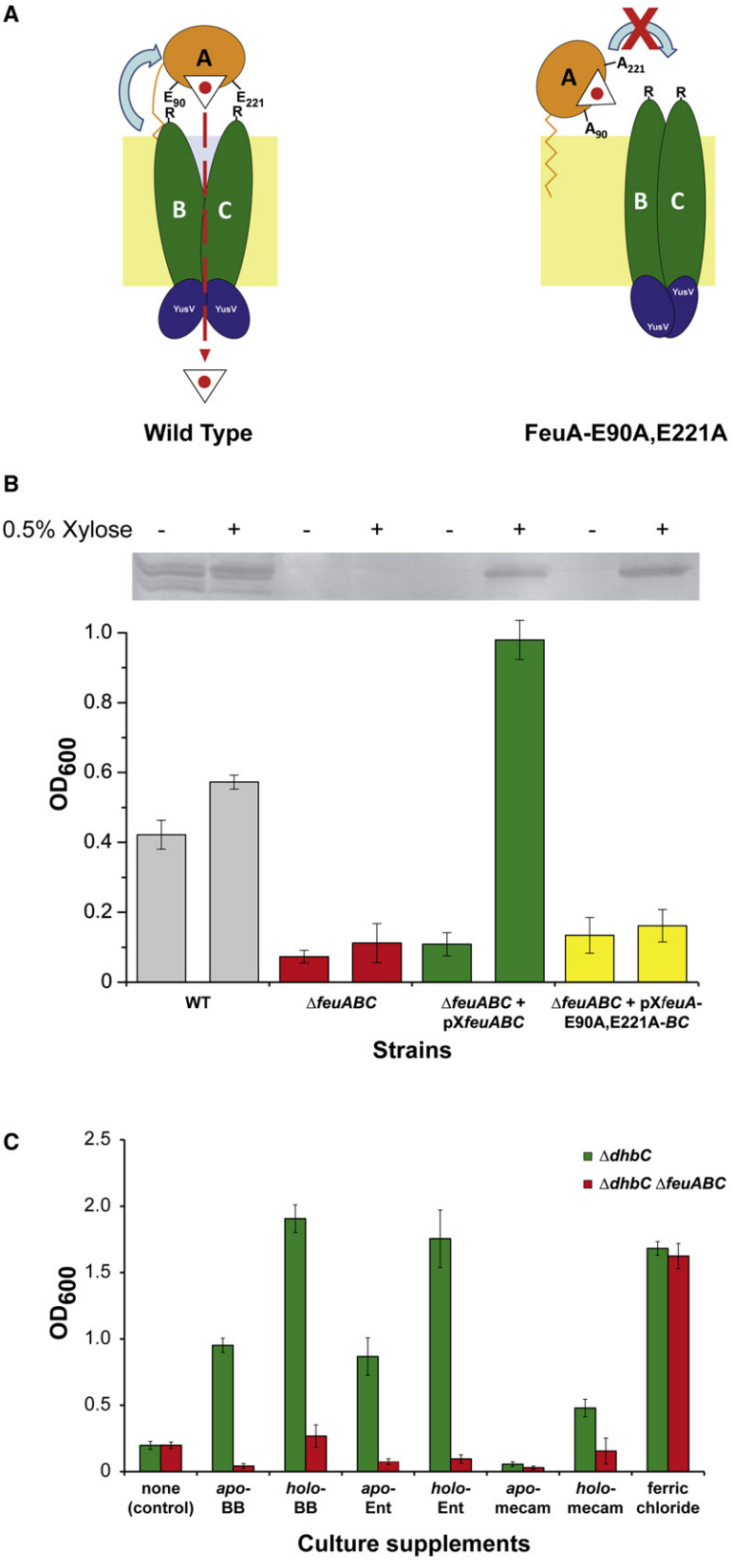

Figure 6. FeuA-FeuBC Interaction Model, Mutational, and Growth Studies

(A) Model for the interaction of the substrate binding protein FeuA and the integral membrane permease FeuBC for ligand translocation into the cytosol. Such interaction is proposed to be mediated by the formation of salt bridges between the two conserved glutamate residues E90 and E221 of FeuA and the arginine residues R59 of FeuB and R53 of FeuC. This allows FeuA to channel the bound ligand into the permease tunnel and, through action of the ATP-hydrolyzing cassettes, to the cytosolic side. FeuA is shown in orange; FeuB and FeuC are shown in green. See also Figure S6 and Table S3.

(B) Growth analysis of *B. subtilis* strains. The final optical density of the strains grown under iron-limited conditions in absence (–) or presence (+) of 0.5% xylose is shown, the standard deviations out of three independent replicates are shown as error bars. *B. subtilis* strains ATCC 21332 (gray), Δ*feuABC* (red), Δ*feuABC* + pX*feuABC* (green) and *B. subtilis* Δ*feuABC* + pX$feuA_{E90A,E221A}$*BC* (yellow) were grown under iron-limited conditions in absence (–) or presence (+) of 0.5% xylose. A western blot using antibodies against FeuA and confirming the expression of FeuA under the control of the xylose promoter in absence (–) or presence (+) of 0.5% xylose is shown above the corresponding bars. Multiple bands observed in ATCC 21332 are most likely degradation products of FeuA. See also Table S4.

(C) Growth analysis of *B. subtilis* Δ*dhbC* mutant (deficient in both 2,3-DHB and BB biosynthesis) and *B. subtilis* Δ*dhbC* Δ*feuABC* double mutant (deficient in both catecholate siderophore biosynthesis and uptake). Cultures were grown in Belitsky minimal medium (in triplicates at 37°C for 12 h) without addition of citrate and without or with different iron source supplements. All indicated supplements were added to a final concentration of 20 μmol L^{-1} at the start of incubation. Standard deviations are shown as error bars.

the mammalian siderophore scavenger siderocalin, where a basic triad coordinates the siderophores by hybrid electrostatic/cation-π interactions (Goetz et al., 2002). The FeuA binding motif seems to perform solely electrostatic interactions with the ligands, possibly due to the need for siderophore release upon transport, which, in contrast, is prevented in the case of siderocalin that shows much higher binding affinities (Abergel et al., 2006; Goetz et al., 2002).

Recently, one more crystal structure of siderocalin (variant K125A) became available in the Protein Data Bank (PDB code: 3CMP, resolution: 2.8 Å) showing three siderocalin-K125A molecules in the asymmetric unit. In two of them, the $[Fe^{III}(Ent)]^{3-}$ complex was present in an undegraded form. Both are distorted and show no high symmetry, neither at the triscatecholate metal center, nor at the trilactone. The carbonyl groups of one molecule point toward the metal center, whereas in the other complex, they point sidewise away from the trilactone. Even our crystal structure at much higher resolution than that of siderocalin-K125A·$[Fe^{III}(Ent)]^{3-}$ showed a $[Fe^{III}(Ent)]^{3-}$ complex with a slightly distorted trilactone ring as well, but with the carbonyl groups pointing away from the metal, thereby resembling the $[V^{I-V}(Ent)]^{2-}$ structure (with inverted stereoconfiguration). Calculations on the free $[Fe^{III}(Ent)]^{3-}$ complex showed no significant energetical preferences for one of the two Λ-configured conformations with the carbonyl groups either pointing toward or away from the metal (Bluhm et al., 2002a). Therefore it seems reasonable that $[Fe^{III}(Ent)]^{3-}$ possesses a certain structural diversity and can be bound in distinct conformations by different binding proteins, which is attended by the sole recognition of the catecholate moieties.

$[Fe^{III}(mecam)]^{3-}$ forms one distinct conformation in complex with FeuA. The monomeric protein-ligand complex which was observed in solution (via size exclusion chromatography), was also present in the crystal structure and differs clearly from the $[\{Fe^{III}(mecam)\}_2]^{6-}$ bridged CeuE dimer (Müller et al., 2006). MM3 calculations indicated a mononuclear structure for the ferric siderophore complex (Hay et al., 2001). The dimeric structure observed for CeuE based on ferric mecam dimerization therefore either may be a crystallization artifact or is the energetic consequence of binding to a differently shaped pocket. The deep and sterically demanding binding cleft of FeuA seems to be the reason for the permitted monomer formation, as a $[\{Fe^{III}(mecam)\}_2]^{6-}$ bridged FeuA dimer would result in steric clashes of the two proteins (Figure S5).

This binding cleft may also be the reason for the inability to bind the related triscatecholate siderophore complex $[Fe^{III}(VB)]^{3-}$. VB features two oxazoline moieties, which are directly attached to two of its three catecholate subunits (Griffiths et al., 1984; Keating et al., 2000). These oxazolines could generate steric hindrance, which hence may prevent binding by the narrow and tight binding pocket of FeuA. As the main fragments which are recognized by the basic triad are the catecholate units, which are also present in VB, the reason of nonbinding by FeuA has to be either the aforementioned steric hindrance or perhaps the inability of $[Fe^{III}(VB)]^{3-}$ to adopt a Λ-configuration.

A sequence alignment of FeuA, CeuE, and other known triscatecholate siderophore binding proteins displayed little homology on the primary structure level. Most conserved residues are typical for all siderophore binding proteins and have been described before (Clarke et al., 2002b). The basic triad is not well conserved, as one could expect at least for the enterobactin binding proteins CeuE and FepB. Furthermore, the overall folds of the FeuA and CeuE binding pockets are quite distinct. The binding pocket of CeuE contributes to its shallower binding of the ligand, as shown in Figure 5. In this light, the evolution of ferric siderophore binding pockets seem to have been independent in different bacterial phyla, and might have been based on one "helical backbone" family ancestor that provided enough plasticity to establish structurally diverse binding environments for functionally similar recognition modes.

To our knowledge, the only siderophore binding protein which has been structurally characterized with more than one ligand is the ferric hydroxymate utilization protein FhuD from *E. coli* (Clarke et al., 2000, 2002a). FhuD complexes with gallichrome, coprogen, the drug desferal, and the siderophore-antibiotic conjugate albomycin show similar cell dimensions and overall structures, which we also observed for the FeuA complexes. Likewise, the major coordination interfaces are located at the iron-binding moieties. Contrary, the binding residues in FhuD undergo significant conformational changes to accommodate the structural features of each siderophore, whereas the basic triad in FeuA shows no outstanding movement. This is presumably due to the fact that the catecholate moieties and their neighboring amide bonds are identical for all three siderophores, which may again explain discrimination of the structurally distant $[Fe^{III}(VB)]^{3-}$.

The rigid binding pocket, which is based on the Λ-mode substrate specificity of FeuA leads to the nearly identical domain movement of the protein, which, in turn, positions the two conserved glutamate residues E90 and E221 conveniently to interact with the basic residues of the transmembrane permease FeuBC. Our mutational studies underline the importance of these two acidic residues for the transport process, which is consistent with previous results on the vitamin B_{12}, ferric citrate, and hydroxamate siderophore transport systems of *E. coli* and *S. aureus*, respectively, while the point mutations did not affect binding of the ligands, which was also observed for the hydroxamate binding protein FhuD (Sebulsky et al., 2003).

The performed uptake studies affirmed the dominant role of the endo- and exogenous triscatecholate siderophores BB and Ent as high-affinity iron sources for *B. subtilis*, while the physiological availability of (ferric) mecam has to be put into question, although the crystallographic and in vitro data confirmed its binding by FeuA. The lower growth promotion by $[Fe^{III}(mecam)]^{3-}$ is corresponding to the higher K_D values obtained in the fluorescence experiments in vitro. The import of $[Fe^{III}(mecam)]^{3-}$ should therefore be possible, but the accessibility of the carried ferric ion in the cytosol could be impaired, which is maybe caused by its nonhydrolyzable backbone. The lower growth of *B. subtilis* Δ*dhbC* under supplementation with *apo*-mecam could further be due to an inhibitory effect of this chelator in a way that mecam is sequestering remaining traces of iron in the medium, which does not become available to the metabolism due to impaired $[Fe^{III}(mecam)]^{3-}$ uptake and/or cytosolic release.

Our experiments could not confirm a proposed secondary uptake system for ferric Ent (Dertz et al., 2006), since deletion of the *feuABC* transporter provided a drastic growth effect,

even if $[Fe^{III}(Ent)]^{3-}$ was supplemented. Later experiments of the group, which originally proposed this secondary transporter, also failed to confirm its presence (Abergel et al., 2009). Nevertheless, a side effect for competitive ferric triscatecholate uptake cannot be completely ruled out, since the characterization of the petrobactin binding protein FpiA (YclQ) also provided some low-affinity binding of $[Fe^{III}(Ent)]^{3-}$ (Zawadzka et al., 2009).

In conclusion, the presented cocrystal structures provide detailed insights into the capture of exogenous triscatecholate siderophores by *Bacillus subtilis* and implied the importance of the binding protein's domain tilt and its exposed opposing glutamates for subsequent transport processes, which has been proved in vitro and in vivo. The deep binding cleft essentially contributes both to high-affinity binding of the substrates, as well as to limited recognition of related substrates possessing unfavorable size or stereoconfiguration.

SIGNIFICANCE

Due to restricted bioavailability, the acquisition of iron is of major importance for microbial survival and for virulence of pathogens. One prominent iron-mobilizing strategy is the secretion of high-affinity iron chelators, so-called siderophores. The inhibition of siderophore uptake systems by artificial antagonists and channeling of siderophore-antibiotic conjugates as "Trojan Horse Antibiotics" are being contemplated as novel antimicrobial tools. Therefore, a precise understanding of the molecular and structural recognition mode of both endo- and exogenous siderophores, as well as synthetic analogs with antagonistic properties is crucial for development of potentially new antibiotics. Substrate binding proteins of Gram-positive bacteria typically possess broader substrate specificities than outer membrane receptors of Gram-negatives, while showing comparable affinities. We investigated the triscatecholate binding protein FeuA from the Gram-positive model organism *Bacillus subtilis* in complex with an exogenous and a synthetic siderophore. The complexes with ferric enterobactin and ferric mecam revealed a similar structural behavior compared with the complex with the endogenous siderophore ferric bacillibactin (Peuckert et al., 2009). Both the binding modes, the overall protein fold and domain movements upon ligand binding were astonishingly conserved throughout these complexes. The overall binding pocket of FeuA is very rigid in size and shape and therefore limited in its substrate tolerance, which is supported by the restriction on Λ-stereoconfigured substrates. The similar domain tilting, representing the largest known movements within class III binding proteins imply their significant importance for the recognition by the transmembrane permease and the subsequent transport process. The highly conserved residues E90 and E221 have been proved to be crucial for this recognition process between binding protein and membrane permease. Another unique feature was the observation of a monomeric form of the ferric mecam complex, which is contrary to the dimer formation by CeuE from *Campylobacter jejuni*, but nevertheless the biological availability of this synthetic iron chelator is impaired and leads to inhibitory effects of growth during iron limitation.

EXPERIMENTAL PROCEDURES

Preparation of Enterobactin, Vibriobactin, and Mecam

H_6-Ent was obtained from the group of Christopher T. Walsh, Harvard Medical School (Fischbach et al., 2005), H_6-VB was purchased from EMC Microcollections (Tübingen, Germany). H_6-mecam was synthesized as described elsewhere (Garrett et al., 1991; Tor et al., 1992). Loading with iron(III) was done as described previously (Miethke et al., 2006).

Cloning, Overexpression, and Purification of Recombinant FeuA and FeuA-E90A,E221A

For expression of FeuA, plasmid pOK01 (Miethke et al., 2006) was used. For cloning of *feuA*-E90A,E221A, pOK01 was used as template and the first point mutation was introduced using Phusion High-Fidelity DNA Polymerase (*Finnzymes*) and the primers feuAE90Afor and feuAE90Arev. After sequencing, the second point mutation was introduced using the primers feuAE221Afor and feuAE221Arev. Sequencing confirmed the correct introduction of both point mutations.

Overexpression of recombinant FeuA and its variant FeuA-E90A,E221A and purification of protein-siderophore complexes was done as described previously (Peuckert et al., 2009).

Crystallization and Data Collection

Crystals of the FeuA·$[Fe^{III}(Ent)]^{3-}$ complex were grown at 18°C by sitting drop vapor diffusion from 600 nl drops. The drops were composed of 300 nl of the crystallization solution (0.1 mol L^{-1} phosphate-citrate [pH 5.2], 34% (v/v) PEG 600) and 300 nl FeuA·$[Fe^{III}(Ent)]^{3-}$ at a concentration of 40 mg ml^{-1}. Crystals of FeuA·$[Fe^{III}(mecam)]^{3-}$ grew under similar conditions using 0.1 mol L^{-1} phosphate-citrate (pH 5.0), 45% (v/v) PEG 300 as crystallization solution. Crystals of diffraction quality grew between 2 days and 2 weeks. For cryocrystallographic analysis the crystals were taken out of the solution and directly flash frozen using liquid nitrogen. All chemicals used for crystallization were of the highest commercially available purity.

Cocrystals with $[Fe^{III}(Ent)]^{3-}$ and $[Fe^{III}(mecam)]^{3-}$ belong both to space group $P12_11$, as do the cocrystals with $[Fe^{III}(BB)]^{3-}$ (PDB code: 2WHY) (Peuckert et al., 2009). Diffraction data sets were collected at a temperature of 100 K at beamline ID14-2 at the European Synchrotron Radiation Facility (ESRF), Grenoble, France and data reduction was performed with the programs XDS and XSCALE (Kabsch, 2010a, 2010b).

Structure Determination and Refinement

Due to the significantly altered cell parameters, a Phaser search (McCoy et al., 2007) was carried out before refinement, using the FeuA·$[Fe^{III}(BB)]^{3-}$ structure (PDB code: 2WHY) as model. TLS and restrained refinement of both structures was performed using REFMAC5 (CCP4, 1994; Murshudov et al., 1997) and COOT (Emsley et al., 2010). At the end of the refinement R_{work}/R_{free} values for FeuA·$[Fe^{III}(Ent)]^{3-}$ converged to 18.5% and 24.3%, respectively and for FeuA·$[Fe^{III}(mecam)]^{3-}$ to 17.8% and 23.7%, respectively. Ligand parameters were calculated using the PRODRG server (Schüttelkopf and van Aalten, 2004) using starting coordinates taken from the Lipocalin 83·$[Ga^{III}(Ent)]^{3-}$ structure for $[Fe^{III}(Ent)]^{3-}$ and from the Hetero-compound Information Centre Uppsala (HIC-Up) (Kleywegt and Jones, 1998) for $[Fe^{III}(mecam)]^{3-}$, respectively. Superposition of the structures and calculation of root mean square deviations was done using the SSM algorithm implemented in COOT.

Circular Dichroism Spectroscopy

CD spectroscopy was carried out in 0.5 cm path length cuvettes, using a J-810 Spectropolarimeter (JASCO) and a protein concentration of FeuA or the complexes with $[Fe^{III}(Ent)]^{3-}$, $[Fe^{III}(mecam)]^{3-}$, $[Fe^{III}(VB)]^{3-}$, or $Fe^{III}(2,3\text{-DHB})_3$ of 2.5 μmol L^{-1} in a buffer containing solely 5 mmol L^{-1} Na-phosphate pH 7.0 for denaturation curves. The measuring range was from 5°C to 95°C using a temperature slope of 1°C min^{-1} and a data pitch of 0.2°C. The monitored wavelength was 222 nm with a bandwidth of 1 nm, a response of 1 s and with standard sensitivity. The measuring conditions for reverse curves were the same; the sample was kept at 95°C for 1 min and then allowed to cool down using the aforementioned temperature slope.

The circular dichroism spectra of $Fe^{III}(2,3\text{-DHB})_3$ and $[Fe^{III}(VB)]^{3-}$ with and without FeuA were recorded at 22.5°C (constant temperature), with a

measuring range from 750 to 300 nm, a band width of 1 nm, a data pitch of 0.2 nm, a response of 1 s and with standard sensitivity. The scanning speed was 50 nm min^{-1} and the presented data are an average of 10 scanning circles. The concentrations of the ferric complexes and the protein were 830 μmol L^{-1} in buffered water (5 mmol L^{-1} Na-phosphate [pH 7.0]).

Fluorescence Spectroscopy

For intrinsic fluorescence spectroscopy a FP-6500 spectrofluorometer (JASCO) was used. Experiments were carried out at 20°C (constant temperature), using an excitation and emission bandwidth of 5 nm each, a response of 0.5 s and low sensitivity. For each measurement series, a protein solution of 5 μmol L^{-1} in 20 mmol L^{-1} Tris-HCl (pH 7.5) was placed in a 1 × 1 cm^2 cuvette, and titrated stepwise with concentrated ligand stock solution. After stirring for 3 min and further 2 min resting, fluorescence was measured by sample excitation at 280 nm and emission monitoring from 300 to 500 nm with a data pitch of 0.5 nm. Emission maxima obtained at 330 nm were used for plotting and binding constant calculation. Therefore, data were set to 100% starting fluorescence intensity and fitted by nonlinear regression analysis (KaleidaGraph 3.52, Synergy Software) using the equation

$$F = \left([P]_t - [L]_t - K_D\right)\frac{f_P}{2} + \left([L]_t - [P]_t - K_D\right)\frac{f_L}{2} + \left([P]_t + [L]_t + K_D\right)\frac{f_{PL}}{2} + \left(f_P + f_L - f_{PL}\right)\sqrt{\frac{\left([P]_t + [L]_t + K_D\right)^2}{4} - [P]_t[L]_t},$$

according to the Law of Mass Action in a one-site binding model, where $[P]_t$ and $[L]_t$ are total protein and ligand concentrations, respectively, f_P, f_L, and f_{PL} are the relative molar fluorescence coefficients of the free protein, the free ligand, and the protein-ligand complex, respectively, and K_D is the dissociation constant. K_D and f_{PL} were set as free parameters, and f_P was set to 100% μM^{-1} according to the starting value.

Mutational and Growth Experiments

Strains and General Methods

Bacterial strains, plasmids, and primers used are listed in Table S4. Antibiotics used for selection of *Bacillus subtilis* strains were used in the following concentrations: chloramphenicol (5 μg ml^{-1}), kanamycin (10 μg ml^{-1}). Antibiotics for selection of plasmid containing TOP10 or XL1Blue strains were used at the following concentrations: ampicillin (100 μg ml^{-1}), kanamycin (50 μg ml^{-1}). Purified FeuA was used for the generation of polyclonal antibodies in rabbits. For this, 500 μg of protein was send to the company (Pineda, Berlin) for immunization. After 110 days of immunization, sera were obtained.

Cloning of feuABC in pX Plasmid and Bacillus subtilis Transformation

The region containing the genes *feuABC* with its cognate ribosomal binding site was amplified from *Bacillus subtilis* ATCC 21332 chromosomal DNA, introducing BamHI (underlined) in the flanking regions. This fragment was cloned into the pCR4Blunt-TOPO vector yielding plasmid pTATCC-*feuABC*. Plasmid pTATCC-*feuABC* was digested with BamHI and the fragment containing the *feuABC* genes was ligated into the pX vector (Kim et al., 1996), yielding plasmid p*XfeuABC*. E90A and E221A variants of FeuA were generated using the plasmid p*XfeuABC*, Phusion DNA polymerase and the primers feuAE90Afor, feuAE90Arev, feuAE221Afor, and feuAE221Arev (modified codons are marked bold and underlined), generating the plasmids p$XfeuA_{E90A}BC$ and p$XfeuA_{E221A}BC$, respectively. A double E90A-E221A FeuA variant was generated from p$XfeuA_{E221A}BC$ using the primers feuAE90Afor and feuAE90Arev, yielding the plasmid p$XfeuA_{E90A,E221A}BC$. The correct sequences of plasmids and the insertion of mutants were confirmed by sequencing (*GATC Biotech*). Plasmids p*XfeuABC* and p$XfeuA_{E90A,E221A}BC$ were linearized with KpnI and used to transform *B. subtilis* BMM110 (Δ*feuABC*) (Miethke et al., 2006). Transformants were selected in antibiotic-containing LB plates. Chromosomal DNA of the transformants was isolated and the integration of *feuABC* and $feuA_{E90A,E221A}BC$ at the *amyE* locus of *B. subtilis* Δ*feuABC* was confirmed by PCR.

In Vivo Analysis of the FeuA-E90A,E221A Variant

Bacillus subtilis strains were grown under agitation (250 rpm) at 37°C. For growth under iron depletion, Belitzky minimal medium (0.5% fructose) without citrate and without iron was used. For *feuABC* expression, cultures of *B. subtilis* at OD_{600} = 0.05 were induced with 0.5% xylose. After 12 hr of growth, the optical density was measured. To detect if the FeuA-E90A,E221A variant was correctly expressed, *B. subtilis* strains were grown in LB at 37°C for 12 hr. Cells were harvested by centrifugation at 13,000 rpm and disrupted by sonication. Twenty-five micrograms of total protein extract was loaded on a 12% SDS-polyacrylamide gel. FeuA was detected using antibodies raised against purified FeuA protein.

Growth Experiments

The strains *B. subtilis* BMM100 (Δ*dhbC*) and *B. subtilis* BMM111 (Δ*dhbC* Δ*feuABC*) (Miethke et al., 2006) were inoculated in Belitsky minimal medium (Stülke et al., 1993) with 0.5% (w/v) glucose as carbon source and without addition of citrate and iron salt and were grown over night to induce iron limitation. Iron-starved cultures were then inoculated to a starting OD_{600} of 0.03 in fresh minimal medium without or with different iron source supplements (all added to 20 μmol L^{-1} final concentration). For each condition, triplicates were prepared and grown in volume scales of 1 ml in round-bottom PE tubes at 37°C and 250 rpm for 12 hr. Optical cell density was monitored spectrophotometrically, and averages of final growth were plotted together with the corresponding standard deviations.

ACCESSION NUMBERS

Coordinates of the FeuA·$[Fe^{III}(Ent)]^{3-}$ and FeuA·$[Fe^{III}(mecam)]^{3-}$ structures have been deposited in the Protein Data Bank with accession codes 2XUZ and 2XV1, respectively.

SUPPLEMENTAL INFORMATION

Supplemental Information includes six figures and four tables and can be found with this article online at doi:10.1016/j.chembiol.2011.05.006.

ACKNOWLEDGMENTS

We gratefully acknowledge the Deutsche Forschungsgemeinschaft for financial support (MA811/23-1). We thank Prof. Lars-Oliver Essen for helpful discussions, Dr. Tobias Klar for support at the ESRF, Detlef Eppers for help with the synthesis of mecam and Tobias Gießen for careful reading of the manuscript. We declare no conflicts of interest.

Received: November 8, 2010
Revised: April 14, 2011
Accepted: May 4, 2011
Published: July 28, 2011

REFERENCES

Abergel, R.J., Wilson, M.K., Arceneaux, J.E., Hoette, T.M., Strong, R.K., Byers, B.R., and Raymond, K.N. (2006). Anthrax pathogen evades the mammalian immune system through stealth siderophore production. Proc. Natl. Acad. Sci. USA *103*, 18499–18503.

Abergel, R.J., Zawadzka, A.M., Hoette, T.M., and Raymond, K.N. (2009). Enzymatic hydrolysis of trilactone siderophores: where chiral recognition occurs in enterobactin and bacillibactin iron transport. J. Am. Chem. Soc. *131*, 12682–12692.

Baker, N.A., Sept, D., Joseph, S., Holst, M.J., and McCammon, J.A. (2001). Electrostatics of nanosystems: application to microtubules and the ribosome. Proc. Natl. Acad. Sci. USA *98*, 10037–10041.

Bao, G., Clifton, M., Hoette, T.M., Mori, K., Deng, S.X., Qiu, A., Viltard, M., Williams, D., Paragas, N., Leete, T., et al. (2010). Iron traffics in circulation bound to a siderocalin (Ngal)-catechol complex. Nat. Chem. Biol. *6*, 602–609.

Bluhm, M.E., Hay, B.P., Kim, S.S., Dertz, E.A., and Raymond, K.N. (2002a). Corynebactin and a serine trilactone based analogue: chirality and molecular modeling of ferric complexes. Inorg. Chem. *41*, 5475–5478.

Bluhm, M.E., Kim, S.S., Dertz, E.A., and Raymond, K.N. (2002b). Corynebactin and enterobactin: related siderophores of opposite chirality. J. Am. Chem. Soc. *124*, 2436–2437.

Borths, E.L., Locher, K.P., Lee, A.T., and Rees, D.C. (2002). The structure of *Escherichia coli* BtuF and binding to its cognate ATP binding cassette transporter. Proc. Natl. Acad. Sci. USA *99*, 16642–16647.

Braun, V., and Braun, M. (2002). Iron transport and signaling in *Escherichia coli*. FEBS Lett. *529*, 78–85.

Braun, V., and Herrmann, C. (2007). Docking of the periplasmic FecB binding protein to the FecCD transmembrane proteins in the ferric citrate transport system of *Escherichia coli*. J. Bacteriol. *189*, 6913–6918.

Bugdahn, N., Peuckert, F., Albrecht, A.G., Miethke, M., Marahiel, M.A., and Oberthur, M. (2010). Direct identification of a siderophore import protein using synthetic petrobactin ligands Angew. Chem. *122*, 10408–10411. Angew. Chem. Int. Ed. Engl. *49*, 10210–10213.

Carrano, C.J., and Raymond, K.N. (1979). Ferric ion sequestering agents. 2. Kinetics and mechanism of iron removal from transferrin by enterobactin and synthetic tricatechols. J. Am. Chem. Soc. *101*, 5401–5404.

CCP4. (1994). The CCP4 suite: programs for protein crystallography. Acta Crystallogr. D Biol. Crystallogr. *50*, 760–763.

Chakraborty, R., Storey, E., and van der Helm, D. (2007). Molecular mechanism of ferricsiderophore passage through the outer membrane receptor proteins of *Escherichia coli*. Biometals *20*, 263–274.

Chipperfield, J.R., and Ratledge, C. (2000). Salicylic acid is not a bacterial siderophore: a theoretical study. Biometals *13*, 165–168.

Clarke, T.E., Ku, S.Y., Dougan, D.R., Vogel, H.J., and Tari, L.W. (2000). The structure of the ferric siderophore binding protein FhuD complexed with gallichrome. Nat. Struct. Biol. *7*, 287–291.

Clarke, T.E., Braun, V., Winkelmann, G., Tari, L.W., and Vogel, H.J. (2002a). X-ray crystallographic structures of the *Escherichia coli* periplasmic protein FhuD bound to hydroxamate-type siderophores and the antibiotic albomycin. J. Biol. Chem. *277*, 13966–13972.

Clarke, T.E., Rohrbach, M.R., Tari, L.W., Vogel, H.J., and Koster, W. (2002b). Ferric hydroxamate binding protein FhuD from *Escherichia coli*: mutants in conserved and non-conserved regions. Biometals *15*, 121–131.

Dertz, E.A., Xu, J., Stintzi, A., and Raymond, K.N. (2006). Bacillibactin-mediated iron transport in *Bacillus subtilis*. J. Am. Chem. Soc. *128*, 22–23.

Ecker, D.J., Matzanke, B.F., and Raymond, K.N. (1986). Recognition and transport of ferric enterobactin in *Escherichia coli*. J. Bacteriol. *167*, 666–673.

Emsley, P., Lohkamp, B., Scott, W.G., and Cowtan, K. (2010). Features and development of Coot. Acta Crystallogr. D Biol. Crystallogr. *66*, 486–501.

Fischbach, M.A., Lin, H., Liu, D.R., and Walsh, C.T. (2005). *In vitro* characterization of IroB, a pathogen-associated *C*-glycosyltransferase. Proc. Natl. Acad. Sci. USA *102*, 571–576.

Garner, B.L., Arceneaux, J.E., and Byers, B.R. (2004). Temperature control of a 3,4-dihydroxybenzoate (protocatechuate)-based siderophore in *Bacillus anthracis*. Curr. Microbiol. *49*, 89–94.

Garrett, T.M., Mcmurry, T.J., Hosseini, M.W., Reyes, Z.E., Hahn, F.E., and Raymond, K.N. (1991). Synthesis and Characterization of Macrobicyclic Iron(III) Sequestering Agents. J. Am. Chem. Soc. *113*, 2965–2977.

Goetz, D.H., Holmes, M.A., Borregaard, N., Bluhm, M.E., Raymond, K.N., and Strong, R.K. (2002). The neutrophil lipocalin NGAL is a bacteriostatic agent that interferes with siderophore-mediated iron acquisition. Mol. Cell *10*, 1033–1043.

Griffiths, G.L., Sigel, S.P., Payne, S.M., and Neilands, J.B. (1984). Vibriobactin, a siderophore from *Vibrio cholerae*. J. Biol. Chem. *259*, 383–385.

Grigg, J.C., Cooper, J.D., Cheung, J., Heinrichs, D.E., and Murphy, M.E. (2010a). The *Staphylococcus aureus* siderophore receptor HtsA undergoes localized conformational changes to enclose staphyloferrin A in an arginine-rich binding pocket. J. Biol. Chem. *285*, 11162–11171.

Grigg, J.C., Cheung, J., Heinrichs, D.E., and Murphy, M.E. (2010b). Specificity of Staphyloferrin B recognition by the SirA receptor from *Staphylococcus aureus*. J. Biol. Chem. *285*, 34579–34588.

Hancock, R.E., Hantke, K., and Braun, V. (1977). Iron transport in *Escherichia coli* K-12. 2,3-Dihydroxybenzoate-promoted iron uptake. Arch. Microbiol. *114*, 231–239.

Hay, B.P., Dixon, D.A., Vargas, R., Garza, J., and Raymond, K.N. (2001). Structural criteria for the rational design of selective ligands. 3. Quantitative structure-stability relationship for iron(III) complexation by tris-catecholamide siderophores. Inorg. Chem. *40*, 3922–3935.

Holmes, M.A., Paulsene, W., Jide, X., Ratledge, C., and Strong, R.K. (2005). Siderocalin (Lcn 2) also binds carboxymycobactins, potentially defending against mycobacterial infections through iron sequestration. Structure *13*, 29–41.

Hvorup, R.N., Goetz, B.A., Niederer, M., Hollenstein, K., Perozo, E., and Locher, K.P. (2007). Asymmetry in the structure of the ABC transporter-binding protein complex BtuCD-BtuF. Science *317*, 1387–1390.

Kabsch, W. (2010a). XDS. Acta Crystallogr. D Biol. Crystallogr. *66*, 125–132.

Kabsch, W. (2010b). Integration, scaling, space-group assignment and post-refinement. Acta Crystallogr. D Biol. Crystallogr. *66*, 133–144.

Kandt, C., Xu, Z., and Tieleman, D.P. (2006). Opening and closing motions in the periplasmic vitamin B_{12} binding protein BtuF. Biochemistry *45*, 13284–13292.

Karpishin, T.B., Stack, T.D.P., and Raymond, K.N. (1993). Stereoselectivity in Chiral Fe(III) and Ga(III) Tris(Catecholate) complexes effected by nonbonded, weakly polar interactions. J. Am. Chem. Soc. *115*, 6115–6125.

Karpowich, N.K., Huang, H.H., Smith, P.C., and Hunt, J.F. (2003). Crystal structures of the BtuF periplasmic-binding protein for vitamin B_{12} suggest a functionally important reduction in protein mobility upon ligand binding. J. Biol. Chem. *278*, 8429–8434.

Keating, T.A., Marshall, C.G., and Walsh, C.T. (2000). Reconstitution and characterization of the *Vibrio cholerae* vibriobactin synthetase from VibB, VibE, VibF, and VibH. Biochemistry *39*, 15522–15530.

Kim, L., Mogk, A., and Schumann, W. (1996). A xylose-inducible *Bacillus subtilis* integration vector and its application. Gene *181*, 71–76.

Kleywegt, G.J., and Jones, T.A. (1998). Databases in protein crystallography. Acta Crystallogr. D Biol. Crystallogr. *54*, 1119–1131.

Krewulak, K.D., Shepherd, C.M., and Vogel, H.J. (2005). Molecular dynamics simulations of the periplasmic ferric-hydroxamate binding protein FhuD. Biometals *18*, 375–386.

Krewulak, K.D., and Vogel, H.J. (2008). Structural biology of bacterial iron uptake. Biochim. Biophys. Acta *1778*, 1781–1804.

Loomis, L.D., and Raymond, K.N. (1991). Solution equilibria of enterobactin and metal enterobactin complexes. Inorg. Chem. *30*, 906–911.

Matzanke, B.F., Ecker, D.J., Yang, T.S., Huynh, B.H., Muller, G., and Raymond, K.N. (1986). *Escherichia coli* iron enterobactin uptake monitored by Mössbauer spectroscopy. J. Bacteriol. *167*, 674–680.

May, J.J., Wendrich, T.M., and Marahiel, M.A. (2001). The *dhb* operon of *Bacillus subtilis* encodes the biosynthetic template for the catecholic siderophore 2,3-dihydroxybenzoate-glycine-threonine trimeric ester bacillibactin. J. Biol. Chem. *276*, 7209–7217.

McCoy, A.J., Grosse-Kunstleve, R.W., Adams, P.D., Winn, M.D., Storoni, L.C., and Read, R.J. (2007). Phaser crystallographic software. J. Appl. Crystallogr. *40*, 658–674.

Miethke, M., Klotz, O., Linne, U., May, J.J., Beckering, C.L., and Marahiel, M.A. (2006). Ferri-bacillibactin uptake and hydrolysis in *Bacillus subtilis*. Mol. Microbiol. *61*, 1413–1427.

Miethke, M., and Marahiel, M.A. (2007). Siderophore-based iron acquisition and pathogen control. Microbiol. Mol. Biol. Rev. *71*, 413–451.

Miethke, M., and Skerra, A. (2010). Neutrophil gelatinase-associated lipocalin expresses antimicrobial activity by interfering with L-norepinephrine-mediated bacterial iron acquisition. Antimicrob. Agents Chemother. *54*, 1580–1589.

Müller, A., Wilkinson, A.J., Wilson, K.S., and Duhme-Klair, A.K. (2006). An $[\{Fe(mecam)\}_2]^{6-}$ bridge in the crystal structure of a ferric enterobactin binding protein. Angew. Chem. *118*, 5256–5260. Angew. Chem. Int. Ed. Engl. *45*, 5132–5136.

Murshudov, G.N., Vagin, A.A., and Dodson, E.J. (1997). Refinement of macromolecular structures by the maximum-likelihood method. Acta Crystallogr. D Biol. Crystallogr. *53*, 240–255.

Ollinger, J., Song, K.B., Antelmann, H., Hecker, M., and Helmann, J.D. (2006). Role of the Fur regulon in iron transport in *Bacillus subtilis*. J. Bacteriol. *188*, 3664–3673.

Peters, W.J., and Warren, R.A. (1968). Itoic acid synthesis in *Bacillus subtilis*. J. Bacteriol. *95*, 360–366.

Peuckert, F., Miethke, M., Albrecht, A.G., Essen, L.O., and Marahiel, M.A. (2009). Structural basis and stereochemistry of triscatecholate siderophore binding by FeuA. Angew. Chem. *121*, 10408–10411. Angew. Chem. Int. Ed. Engl. *48*, 7924–7927.

Raymond, K.N., and Carrano, C.J. (1979). Coordination chemistry and microbial iron transport. Acc. Chem. Res. *12*, 183–190.

Schrödinger, LLC (2010). The PyMOL Molecular Graphics System, Version 1.3r1.

Schüttelkopf, A.W., and van Aalten, D.M. (2004). PRODRG: a tool for high-throughput crystallography of protein-ligand complexes. Acta Crystallogr. D Biol. Crystallogr. *60*, 1355–1363.

Sebulsky, M.T., Shilton, B.H., Speziali, C.D., and Heinrichs, D.E. (2003). The role of FhuD2 in iron(III)-hydroxamate transport in *Staphylococcus aureus*. Demonstration that FhuD2 binds iron(III)-hydroxamates but with minimal conformational change and implication of mutations on transport. J. Biol. Chem. *278*, 49890–49900.

Sharff, A.J., Rodseth, L.E., Spurlino, J.C., and Quiocho, F.A. (1992). Crystallographic evidence of a large ligand-induced hinge-twist motion between the two domains of the maltodextrin binding protein involved in active transport and chemotaxis. Biochemistry *31*, 10657–10663.

Shi, R., Proteau, A., Wagner, J., Cui, Q., Purisima, E.O., Matte, A., and Cygler, M. (2009). Trapping open and closed forms of FitE: a group III periplasmic binding protein. Proteins *75*, 598–609.

Stülke, J., Hanschke, R., and Hecker, M. (1993). Temporal activation of β-glucanase synthesis in *Bacillus subtilis* is mediated by the GTP pool. J. Gen. Microbiol. *139*, 2041–2045.

Tor, Y., Libman, J., Shanzer, A., Felder, C.E., and Lifson, S. (1992). Chiral siderophore analogs - enterobactin. J. Am. Chem. Soc. *114*, 6661–6671.

Ward, J.J., McGuffin, L.J., Bryson, K., Buxton, B.F., and Jones, D.T. (2004). The Dros. Inf. Serv.OPRED server for the prediction of protein disorder. Bioinformatics *20*, 2138–2139.

Zawadzka, A.M., Kim, Y., Maltseva, N., Nichiporuk, R., Fan, Y., Joachimiak, A., and Raymond, K.N. (2009). Characterization of a *Bacillus subtilis* transporter for petrobactin, an anthrax stealth siderophore. Proc. Natl. Acad. Sci. USA *106*, 21854–21859.